DESIGN CONSIDERATIONS FOR ION MICROTHRUSTERS

G. J. Yashko†, G. B. Giffin†, D.E. Hastings††
Massachusetts Institute of Technology
Cambridge, Massachusetts

Abstract

This paper explores, from a numerical perspective, the factors that affect the performance of ion engines as their size is reduced several orders of magnitude. A previously developed code used to predict performance in traditional ring-cusped ion engines is used to analyze the effect of scaling engines with cylindrical chambers. It was shown that, although desirable, magnetic fields can not be scaled inversely proportional to the chamber scale. Even the best practical permanent magnets provide little electron or ion containment below ~1 mm chamber sizes. At those scales the fraction of ions which reach the beam is essentially the ratio of the chamber exit area to the total chamber area. Application of these findings to linear ion microthruster design indicate that beam ion production costs tends to decrease as the number chambers decreases for a given thrust level. Further, for a given number of chambers beam ion cost increases as length increases.

Nomenclature

A_g = thruster grid area, m^2
C_o = primary electron utilization factor, A^{-1}
e = electric charge, 1.6×10^{-19} C
f_B = fraction of ions extracted
f_C = fraction of ion current produced that goes to cathode potential surfaces
g_o = gravitational acceleration, 9.8 m/s^2
J_B = ion beam current, A
l_e = primary electron containment length, m
m_e = mass of electron, kg
m_i = mass of propellant ion/neutral atom, kg
$\dot{m}$ = propellant mass flow rate per chamber, Aeq
n_o = neutral atom density, kg/m^3
n_m = Maxwellian electron density $\#/m^3$
n_p = primary electron density, $\#/m^3$
n_+ = ion density, $\#/m^3$
r_L = Larmor radius, m
T_e = electron temperature, eV
V_D = discharge voltage, V
v_B = Bohm velocity, m/s
v_o = neutral velocity, m/s
v_p = primary electron velocity, m/s
ε_B = average beam ion energy costs, eV
ε_o = permittivity of free space, C^2/Nm^2
ε_P^* = minimum plasma ion energy costs, eV
λ = mean free path, m
λ_D = Debye length, m
ϕ_i = grid transparency to ions
ϕ_o = grid transparency to neutrals
η_u = propellant utilization efficiency
$\sigma_{e\text{-}i}$ = elastic collision cross section for e-i m^3
$\sigma_{e\text{-}n}$ = elastic collision cross section for e-n, m^3
σ_t = inelastic collision cross section for e-n, m^3

† Graduate Research Assistant
†† Professor of Aeronautics and Astronautics

Copyright © 1997 by the Electric Rocket Propulsion Society. All rights reserved.

1 INTRODUCTION

Future spacecraft may employ microthrusters for missions requiring precise, low-thrust firings. These missions may include precision station-keeping of separated spacecraft forming a large sparse aperture, control of large flexible structures such as deployable antennas or solar arrays, or as the main propulsion system for microsatellites.

This paper explores, from a numerical perspective, the factors that affect the performance of ion engines as their size is reduced several orders of magnitude. A code developed by Arakawa to predict performance in traditional ring-cusped ion engines is used to analyze the effect of scaling engines with cylindrical chambers. Modifications to the code were made in order to analyze ion microthruster concepts consisting of linear chambers.

The code is discussed first with an emphasis on the formulations used to simulate particle behavior within the chamber. This is important because of the assumption in subsequent analysis that the physics remain the same at smaller scales. Next, an argument is outlined as to how thruster parameters such as mass flow rate and discharge voltage should change as thruster size is scaled. The effect on performance of scaled cylindrical ion thrusters is then presented. Finally, preliminary design considerations affecting the performance of the linear ion microthruster concept are highlighted.

2 OVERVIEW OF NUMERICAL MODEL

The performance of an ion thruster is gauged by the power required to produce, but not accelerate, an ion which eventually becomes part of the beam. The average energy cost to produce a single beam ion, ε_B, is a key parameter in the measure of the thrusters performance. To produce a more efficient thruster it is necessary to reduce the value of ε_B while maintaining a high propellant utilization. Brophy[1] developed a model for predicting ε_B in ring and line cusp ion thrusters.

The average beam ion energy cost is given as

$$\varepsilon_B = \frac{\varepsilon_P^*}{f_B\left\{1-\exp\left[-C_o\dot{m}(1-\eta_u)\right]\right\}} + \frac{f_C}{f_B}V_D \quad (1)$$

where $C_o = 4\sigma_o l_e / e v_o A_g \varphi_o$ and $\dot{m}$ is the mass flow rate per chamber in Aeq/s. Eq. (1) indicates that it is desirable to maximize the value of the primary electron containment length, l_e, in order to reduce the power needed to create beam ions. In other words, the longer an average primary electron remains in the chamber before being lost to the anode, the more effective ionizer it is and the more efficient the thruster will be. Ring and line cusped ion engines increase l_e by employing magnets which cause the electrons to spiral around magnetic field lines.

Eq. (1) also indicates that it is desirable to maximize the fraction of ions reaching the beam, f_B, and minimize the fraction of ions reaching cathode potential surfaces, f_C. In a well-designed chamber, the presence of a magnetic field tends to contain the primary electrons near the center of the chamber. Because a higher percentage of ionizations occur near the chamber center and the ion's ability to diffuse across field lines is hindered, f_B increases and f_C decreases yielding improved performance.

The analytic code, developed by Arakawa[2], is a collection of programs which calculates the parameters listed in the formulation for average beam ion production costs, Eq. (1). The outline of the calculation procedure, taken from Ref. 2, is shown in Figure 1. Given the geometry and materials making up the chamber's walls and magnets, the magnetic field analysis program computes magnetic vector potentials within the chamber. With the magnetic fields inside the chamber known, the Monte Carlo simulation computes the electron confinement length, l_e, and primary electron density distribution, $n_p(r,z)$. Using $n_p(r,z)$, along with chosen values for ion and neutral grid transparencies and an initial estimate of electron temperature, the fraction of ions traveling to cathode potential surfaces, f_C, and extracted into the beam, f_B, can be calculated. These parameters are then used to recalculate the electron temperature from conservation of energy. The procedure is repeated with a revised estimate of electron temperature until the initial and final values agree. The results are then substituted into Brophy's discharge performance model, Eq. (1) to give average ion energy cost at the chosen value of propellant utilization.

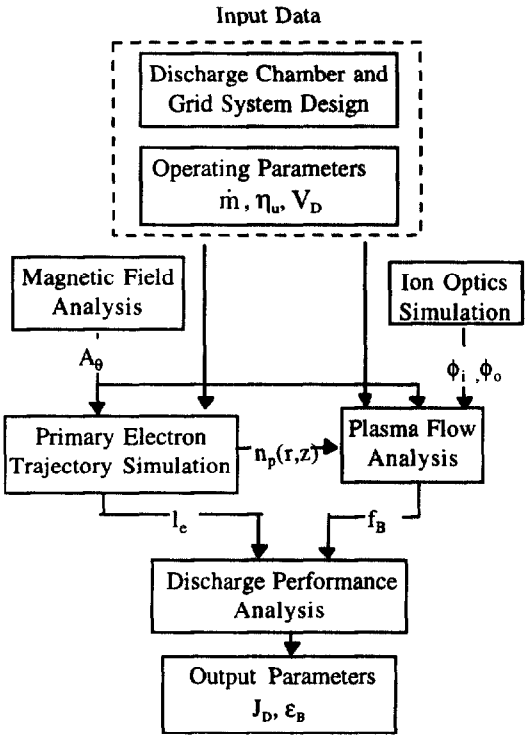

Figure 1 - Arakawa code calculation procedure.

Although the original magnetic field analysis program has produced valid fields in the past[2], the current version of the code generated physically impossible results. A typical characteristic of these flawed results were flux density values equal to zero at all points along the centerline. A commercial package, MAGNETO[3], was therefore, used to perform the magnetic field analysis.

The next section examines how each of the input parameters to the Arakawa code should scale in order to maintain the same discharge chamber performance as chamber size is reduced.

3 SCALING ARGUMENT

As the size of the thruster is decreased, the chamber exit area will scale as $A_g \sim L^2$ where L is a characteristic length. To maintain the same energy cost per beam ion as chamber size is scaled, Eq. (1) suggests that the primary electron confinement length and mass flow rate should scale as $l_e \sim L$ and $\dot{m} \sim L$.

Maintaining l_e proportional to a characteristic chamber length should be a matter of keeping the same "degree of particle interaction" between the electrons, neutrals, and ions. Ideally this would be accomplished by altering the magnetic field strength and particle densities so that the Larmor radius and mean free paths scale as L. Magnetic field strength, B, and Larmor radius are related by

$$B = \frac{m_e v_p}{e r_L} \tag{2}$$

Eq. (2) implies that $B \sim 1/L$ since m_e and e are constants and v_p is proportional to $\sqrt{V_D}$ which is assumed invariant. The mean free paths for elastic collisions of electrons with neutrals and ions, inelastic ionizing collisions with neutrals, and electron-wave interactions due to plasma oscillations are, respectively

$$\lambda_{e-n} = \frac{1}{n_o \sigma_{e-n}} \tag{3}$$

$$\lambda_{e-i} = \frac{4.5 \times 10^{16} V_D^2}{n_+} \tag{4}$$

$$\lambda_{ion} = \frac{1}{n_o \sigma_+} \tag{5}$$

$$\lambda_{anom} = 2\pi \left(\frac{2\varepsilon_o}{e} \frac{V_D}{n_+} \right)^{1/2} = 2\pi \lambda_d \tag{6}$$

where $n_+ = n_p + n_m$ since a primary electron is assumed to become a secondary electron after colliding with a neutral to form an ion. For the mean free paths to scale as L, Eqs. (3) through (5) require that the neutral and ion densities scale as $n_o \sim 1/L$ and $n_+ \sim 1/L$. With $n_+ \sim 1/L$, Eq. (6) indicates that λ_{anom} does not scales as L but as $\sqrt{L}$ with the result being that electron wave interactions occur less frequently as size is reduced.

That $n_o \sim 1/L$ is consistent with $\dot{m} \sim L$ since

$$n_o = \frac{4\dot{m}(1-\eta_u)}{m_i v_n A_g \phi_o} \tag{7}$$

That $n_+ \sim 1/L$ is consistent with $\dot{m} \sim L$ since

$$J_B = \dot{m}\eta_u = 0.61\left(n_+ v_B A_g \phi_i\right) \tag{1}$$

where $A_g \sim L^2$ and v_B is proportional to $\sqrt{T_e}$ which is assumed invariant. It is also desired that the propellant utilization, η_u, remain invariant. Propellant utilization can be represented as

$$\eta_u = 1 / \left(1 + \frac{0.15 e \varepsilon_p^* v_B A_g^2 \ \phi_i \phi_o \bar{c}_n \left(1 + \frac{n_p}{n_m}\right)}{J_B f_B V_D v_p (Vol) \sigma_T \left(\frac{n_p}{n_m}\right)} \right) \tag{2}$$

where $v_p \sim \sqrt{V_D}$, $\bar{c}_n \sim \sqrt{T_n}$ and $v_B \sim \sqrt{T_e}$ and so remain invariant given the assumptions that Te and V_D are invariant. Additionally, $A_g \sim L^2$, $J_B \sim L$ and $Vol \sim L^3$. η_u, then, will remain invariant only if the ratio of primary to secondary electrons, n_p/n_m, and baseline energy cost per ion, ε_p^*, are invariant. n_p/n_m and ε_p^* can be calculated, respectively, as

$$\frac{n_p}{n_m} = \left(\frac{\bar{c}_e}{v_p}\right) \left(\frac{U^+ + \varepsilon_m + U_{exc}\left(\frac{\bar{\sigma}_{exc}}{\bar{\sigma}_+}\right)}{(V_D - \varepsilon_m)\left(\frac{\sigma_T}{\bar{\sigma}_+}\right) - \left(\frac{\sigma_+}{\bar{\sigma}_+}\right)\left(U^+ + \varepsilon_m\right) - \frac{\sigma_{exc}}{\bar{\sigma}_+}} \right) \tag{3}$$

and

$$\varepsilon_p^* = \frac{V_D\left(\frac{\sigma_T}{\sigma_+}\right)}{1 + \frac{n_m}{n_p}\frac{\bar{c}_e}{v_p}\frac{\bar{\sigma}_+}{\sigma_+}} \tag{4}$$

Therefore, n_p/n_m and ε_p will remain invariant if $\bar{c}_e$ is invariant. $\bar{c}_e$ is given by

$$\bar{c}_e = \sqrt{\frac{8}{\pi}\frac{e}{m_e} T_e} \tag{5}$$

indicating that it is consistent for η_u and T_e to simultaneously remain invariant as thruster scale is reduced.

A 10 cm diameter ion thruster typically utilizes a 0.1 T magnetic field. Scaling the thruster to a diameter of approximately 1 cm requires a 1 T magnetic field which may be achieved using rare-earth ceramic magnets. Achieving the 10 T field strength necessary for a 1 mm size microthruster would presumably require superconducting wire solenoids to avoid ohmic losses (and subsequent thermal issues) in the wires.

4 SCALING OF CYLINDRICAL CHAMBERS

Given that the structural, material, and power resources required to produce magnetic field strengths of several tesla in the chamber of an ion microthruster are not yet available, the effect of scaling a chamber while holding the permanent magnet surface strength constant was investigated. Many of the relationships presented in section 2 will not hold since the magnetic flux density will not scale proportional to 1/L.

The analytic code described in section 2 was used to determine the effect that scaling has on discharge chamber performance. A 7cm ion thruster developed at Colorado State University was chosen as a baseline because it has undergone experimental testing and numerical simulation. The chamber geometry with corresponding field lines and flux density contours are shown in Figure 2 and Figure 3 respectively. Magnetic flux density was held at 1200 G at the magnet surfaces for all cases.

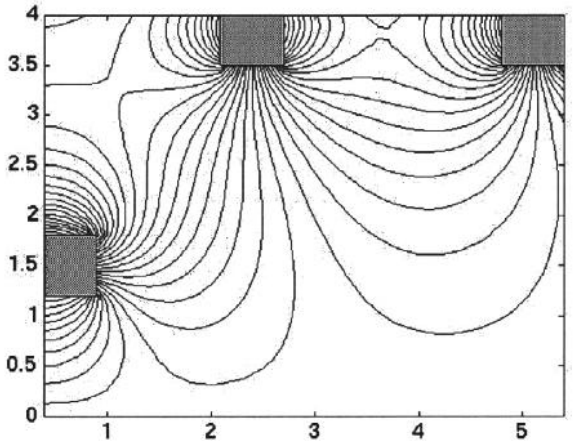

Figure 2- 7cm CSU magnetic potential contours.

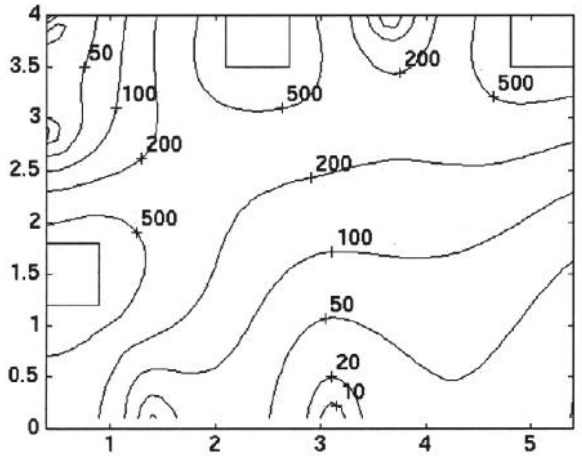

Figure 3- 7cm CSU flux density contours.

Figure 4 shows beam ion production cost, ε_B, as a function of propellant utilization for cylindrical chamber diameters ranging from 7cm to 0.07cm. Despite best efforts, the values for the 7cm case differ significantly from those obtained in Ref. 2. The higher ε_B calculated for this paper are due to a lower fraction of ions reaching the beam (f_B=0.21 vs. 0.29 in Ref. 2). This discrepancy is probably due to differences in the magnetic field as generated by MAGNETO and Arakawa's magnetic field analysis program. Although the values of ε_B in this analysis do not agree with experimental data, it is still possible to identify the factors influencing ε_B as chamber size is scaled.

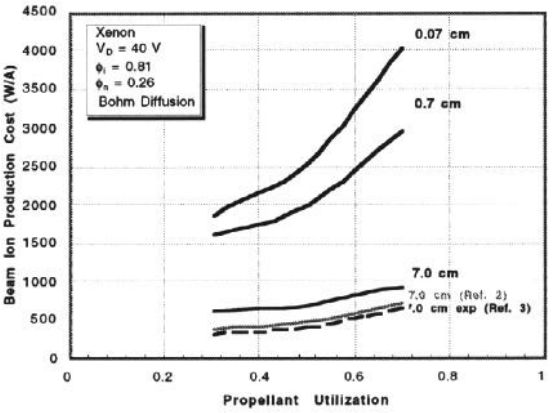

Figure 4- ε_B vs. η_u.

The results of scaling the 7cm CSU ion thruster as generated by the Arakawa code are listed in Table 1. How each parameter scales with the characteristic length is also shown. The neutral density scales as 1/L as expected due to the scaling of mass flow rate as L. Due to the lack of a magnetic field the primary electron confinement length scales greater than L. This results in proportionately less ionization so that ion density scales less than proportional to L. The equilibrium temperature does not, therefore, remain invariant but increases slightly as the thruster is scaled down.

Figure 5 shows the distribution of primary electrons in the 7cm chamber. The peak electron density occurs at the position of the cathode. As shown in the figure, the magnetic field tends to contain the primary electrons near the chamber center. Ionizations will then also tend to occur near the chamber center resulting in a plasma density distribution as shown in Figure 6. A large fraction of ions, f_B, reaches the beam tending to improve performance (see Table 1).

Table 1 - Scaling of 7cm CSU ion thruster (η_u=0.7)

	units	L	0.1L	0.01L	Scales as
d_B	m	0.07	0.007	0.0007	L
$\dot{m}$	$(Aeq)^{-1}$	0.15	0.015	0.0015	L
min r_L	m	1.8e-4	1.8e-4	1.8e-4	1
λ_{e-n}	m	1.01	0.101	0.0101	L
λ_{e-i}	m	334.0	34.1	3.44	~L
λ_{ion}	m	4.7	0.47	0.047	L
λ_{anom}	mm	9.0e-4	2.8e-4	09.1e-5	$\sqrt{L}$
l_e	m	2.09	0.076	0.00629	-
C_o	$(Aeq)^{-1}$	12.5	46.4	376.0	-
n_o	$10^{18}/m^3$	4.76	47.6	476.0	1/L
n_+	$10^{18}/m^3$	0.130	1.25	12.7	~L
n_p	$10^{18}/m^3$	0.0206	0.310	3.53	-
f_B	unitless	0.21	0.14	0.12	-
f_C	unitless	0.79	0.86	0.88	-
T_e	eV	3.61	3.78	3.82	-
ε_p	W	70.4	72.5	73.1	-
ε_B	W	940	2963	4029	-

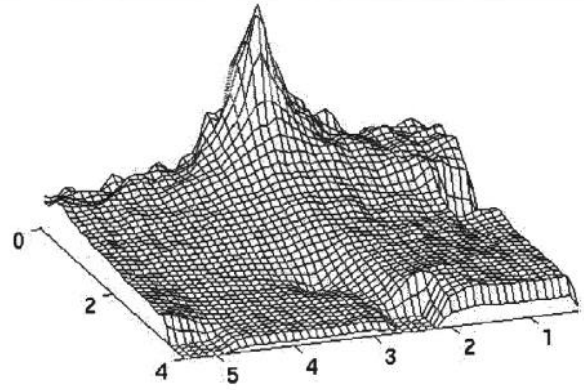

Figure 5- Primary electron densities for 7cm chamber.

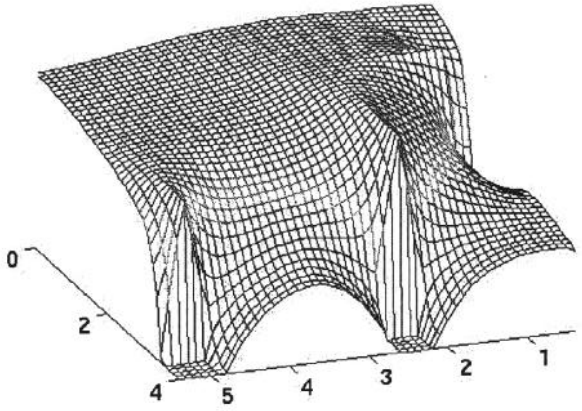

Figure 6- Plasma densities for 7cm chamber.

Because the strength of the magnetic field can not be increased as chamber size is scaled down, the Larmor radius increases relative to the size of the chamber. The primary electrons can easily cross field lines reaching all regions of the chamber. For the 0.7cm and 0.07cm cases then, ionization occurs more uniformly. The resulting plasma density distributions are shown in Figure 7 and Figure 8. A lower fraction of ions reach the beam leading to decreased performance as compared to the 7cm case. For the cylindrical geometry analyzed here the ratio of exit area to total chamber surface area is 0.11. It is clear from Table 1 that as chamber size is scaled down the fraction of ions reaching the beam approaches the 0.11 value. This indicates that the magnetic field does not significantly confine the electrons or ions at the smallest scales.

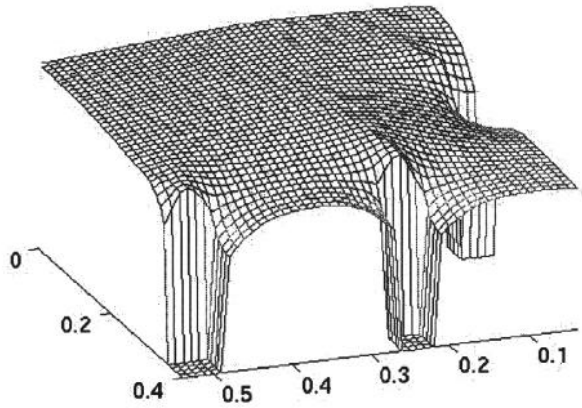

Figure 7 - Plasma densities for 0.7cm chamber.

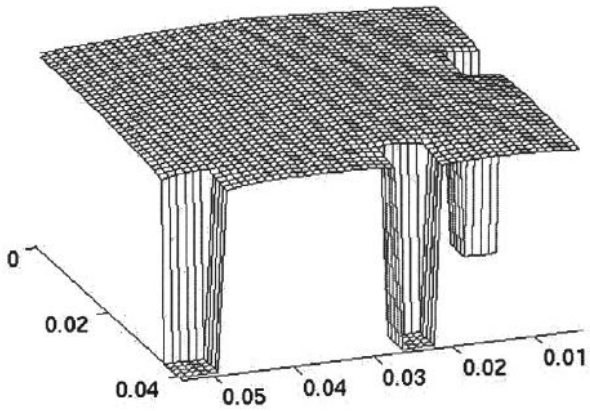

Figure 8- Plasma densities for 0.07cm chamber.

5 ANALYSIS OF LINEAR CHAMBERS

The results of the previous section demonstrate that as size is scaled down several orders of magnitude the plasma density becomes uniform. Hence, the fraction of ions which reach the beam may be taken as the ratio of the chamber exit area to the total chamber surface area for the multi-chamber configuration shown in Figure 9. The primary electron trajectory simulation was modified to accommodate rectilinear chamber geometries. The magnetic field was again calculated using MAGNETO with the results shown in Figures 10 and 11. Flux density at the surface of the magnets was maintained at 1200 G. It was found that the primary electron confinement length, valued at about 1.06 cm, was independent of many of the input parameters. As expected, the confinement length did not depend on the chamber length since the magnetic field profile does not vary down the channel.

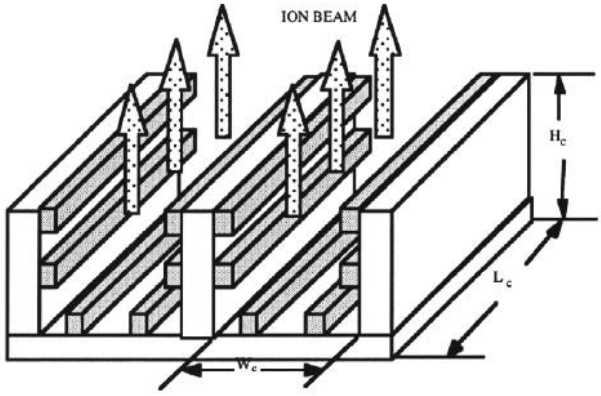

Figure 9 - Linear geometry examined.

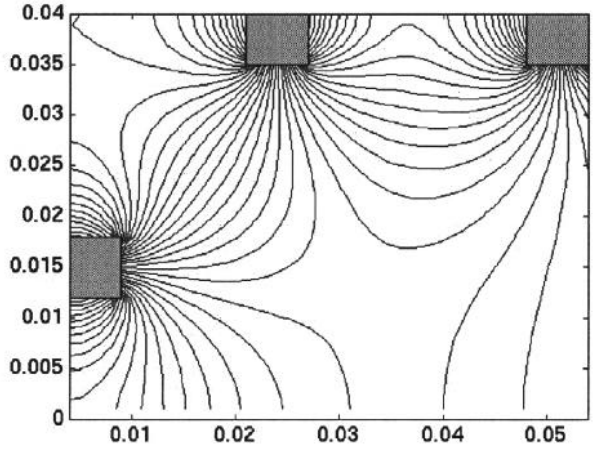

Figure 10 - Linear geometry magnetic field lines.

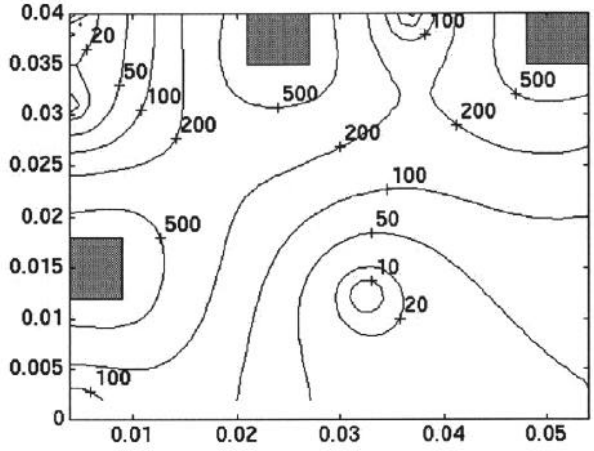

Figure 11 - Linear geometry flux density contours.

Since the beam fraction may be taken as the simple exit area to total chamber surface area ratio, Eq. (1) could be employed to determine beam ion production cost without plasma flow simulation. Figure 12 presents the methodology used to analyze the performance of the linear configuration. Assuming a total thrust, F_{tot}, of 5 mN and a specific impulse of 3300s, the total mass flow rate is 0.162 A-eq. Knowing the chamber width, length and grid spacing, the allowable mass flow rate per chamber can be calculated from the Child-Langmuir 1-D space charge limit (SCL) equation. The mass flow per chamber can be divided into the total mass flow for the thruster yielding the required number of chambers. Values of T_e and ε_p^* were determined through an iterative process based on energy equilibrium in the discharge chamber.

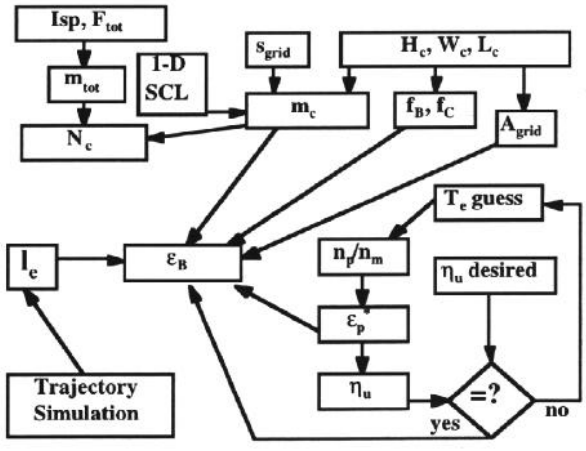

Figure 12 - Linear analysis methodology.

Figure 13 shows the variation of beam ion production cost with chamber length for the case where transparencies to ions and neutrals are 0.81 and 0.26,

respectively. Grid separation was limited to values greater then 10 microns. The height and width of all chambers remained constant at 0.05 cm and 0.07 cm, respectively. At a chamber length of 0.07 cm, 14 chambers were required to satisfy space charge limitations. As length increased, fewer chambers were required to provide the necessary mass flow rate. Beam ion production costs tends to decrease as the number chambers decreases. With fewer chambers the increased mass flow rate in each chamber offsets the decrease in grid area (see Eq. (1)). For a given number of chambers, however, beam ion production costs increase as length increases. This is due to an increase in grid area with no increase in mass flow rate per chamber.

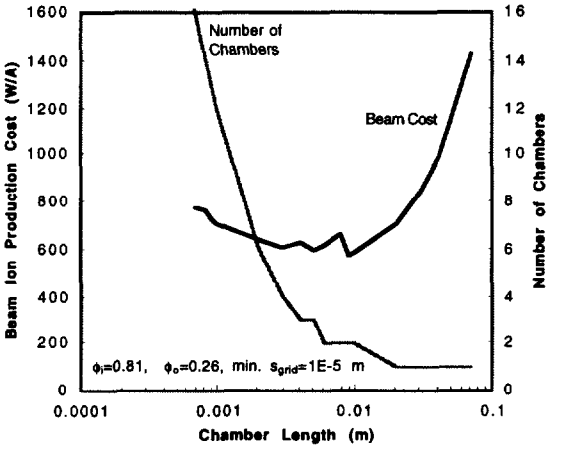

Figure 13 - Relationship between beam cost and number of chambers.

Some microthruster concepts have foregone an exit grid due to potential manufacturing difficulties. Instead, they provide ion acceleration via electric fields applied from the chamber walls. Figure 14 presents the case of no grid (i.e. ϕ_i=1 and ϕ_o=1). The lower neutral density in the chamber results in a jump in beam ion production cost. This was investigated for two different minimum grid spacings and demonstrates that performance improves with decreasing grid spacing. Smaller grid spacings allow higher mass flow rates and therefore higher neutral densities in the chamber.

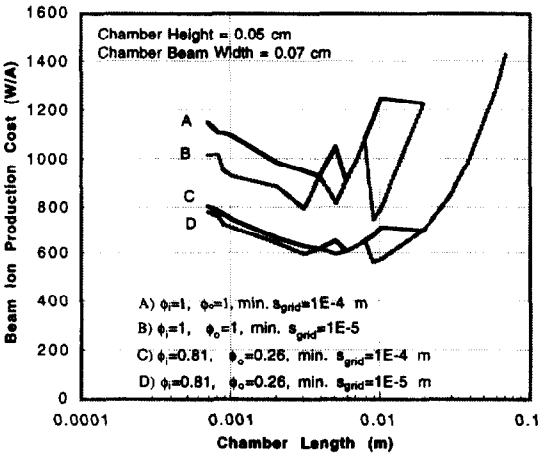

Figure 14- Beam ion energy cost vs. chamber length for several grid transparencies and spacings.

6 SUMMARY AND CONCLUSIONS

This paper examined possible design considerations for ion microthrusters. It was shown that, although desirable, magnetic fields can not be scaled inversely proportional to the chamber scale. Even the best practical permanent magnets provide little electron or ion containment below ~1 mm chamber sizes. At those scales the fraction of ions which reach the beam is essentially the ratio of the chamber exit area to the total chamber area. Application of these findings to linear ion microthruster design indicate that beam ion production costs tends to decrease as the number chambers decreases for a given thrust level. Further, for a given number of chambers beam ion cost increases as length increases.

References

1. Brophy, J.R., Wilbur, P.J., "Simple Performance Model for Ring and Line Cusp Ion Thrusters" AIAA Journal pp. 1731-1736, 23 No. 11, November 1985.

2. Arakawa, Y., Ishihara, K., "A Numerical Code for Cusped Ion Thrusters." IEPC-91-118, 22nd International Electric Propulsion Conference, Oct. 14-17, 1991, Viareggio, Italy.

3. MAGNETO by Integrated Engineering Software Inc. 46-1313 Border Place Winnipeg, Manitoba, Canada R3H0X4, http://www.integrated.mb.ca/ies

4. Vaughn, J.A., and Wilbur, P.J., "Ring Cusp/ Hollow Cathode Discharge Chamber Performance Studies." IEPC-88-064, 20th International Electric Propulsion Conference, Garmisch-Partenkirchen, W. Germany, Oct. 3-6, 1988.